Exploring Computer-based Rock Mass Characterization

Louis N.Y. WONG & K.K. CHAN,

Department of Earth Sciences, The University of Hong Kong

S.N. GOH, Ivan H.H. CHAN & Regis L.G. CHEE

Geotechnical Engineering Office, Civil Engineering and Development Department, HKSAR Government

doi: https://doi.org/10.21467/proceedings.171.25

ABSTRACT

The precision and representativeness of manual rock mass characterization result are often limited by site constraints or practices due to accessibility, safety, time, and unfavourable environmental conditions. In this study, we have formulated a computerized workflow for rock mass characterization by adopting the NGI Q-system, with the aid of laser scanning that could be easily deployed on underground construction sites. This study also explores the application of artificial intelligence, specifically deep learning, in the proposed workflow for rock mass characterization based on the relationship between Rock Quality Designation (RQD) and number of discontinuity sets (J_n) and the block shapes and sizes. In order to effectively train the deep learning model, we propose a novel technique called Synthetic Rock Mass Point Cloud (SRMPC) to generate point clouds model of rock mass with varying RQD and discontinuity sets. SRMPC utilizes an implicit approach with signed distance functions to model rock mass geometry and employs the sphere tracing technique for efficient point cloud generation. A synthetic dataset comprising 35 classes of RQD and J_n combinations was created to train and test a deep learning model, PointNet++ (Qi et al., 2017), for classification. The deep learning model exhibited a certain ability to identify the features of the synthetic rock mass with varying RQD, but faced challenges in distinguishing rock masses with similar RQD and discontinuity sets. To address this problem, a revised 20-class classification model was developed and trained, resulting in improved accuracy.

1 INTRODUCTION

1.1 Background

Rock mass characterization is essential to rock support design of underground openings. However, site constraints, accessibility, unfavorable environmental conditions, and procedures related to safety and time often limit the precision and representativeness of rock mass characterization in conventional practice. For example, measuring joint orientations at a tunnel's crown using a compass is challenging, if not impracticable. This study explored the application of remote sensing techniques and computer vision for rock mass characterization, primarily on digitizing the process of rock mass classification, to enhance safety and cost-effectiveness of underground construction in rock.

One of the most commonly used rock mass classification systems in Hong Kong – the NGI Q-system by Barton et al. (1974), updated by NGI (2015) has five out of six parameters (i.e. Rock Quality Designation, Joint set number, Joint roughness number, Joint alteration number and Joint water reduction factor) characterizing various discontinuity properties in a rock mass. The successful applications of the NGI Q-system in Hong Kong have been recognized by Barton (2015) and play a pivotal role in the local hard rock tunnelling and cavern engineering practices.

Remote sensing techniques such as photogrammetry and laser scanning can capture point clouds of rock mass with sufficient information for interpreting RQD and Joint set number (J_n). Laser scanners, particularly handheld/mobile laser scanners, are found to be more suitable for underground construction. However, capturing other parameters, including Joint roughness number (J_r), Joint alteration number (J_a) and Joint water reduction factor (J_w) from the point clouds data is still challenging due to the resolution and different nature of the measurements.

This study focused on streamlining the process of characterization of RQD and J_n, using point cloud data, since these two parameters are critical to the result of rock mass characterization and could vary greatly within

Proceedings DOI: 10.21467/proceedings.171; Series: AIJR Proceedings; ISSN: 2582-3922; ISBN: 978-81-970666-7-2

a small space. Moreover, these parameters can be interpreted from point cloud data with relatively high accuracy. The remaining parameters (i.e. J_r, J_a, J_w and stress reduction factor) generally relate to larger-scale geological conditions and vary less when compared to RQD and J_n. Obtaining these parameters through engineering geologists' field observations is considered more efficient and reliable.

1.2 Related work

In recent years, many researchers have investigated extracting discontinuity planes from point clouds (e.g. Chen et al., 2016; Gigli & Casagli, 2011; Riquelme et al., 2014; etc). Theoretically, RQD and J_n can be determined if all discontinuities are perfectly outlined in a point cloud. However, characterizing RQD or J_n using these existing methods is typically not reliable enough for actual construction. For example, wavy discontinuity planes are often split into multiple planes by these algorithms. Moreover, existing analytical methods require users to determine multiple parameters, such as minimum angular difference between two planes. Obtaining the best result necessitates careful calibration and tuning of these parameters to accommodate the site and the geology, which can be time-consuming (So et al., 2021).

One potential solution to overcome the limitations of these existing methods is deep learning. Recent research, such as PointNet++ by Qi et al. (2017), has demonstrated the capability of deep learning to perform tasks including classification and segmentation of point cloud data. We noticed that an experienced mapping personnel can roughly describe rock mass quality based on the overall appearance without delineating every discontinuity. Deep learning has the potential to acquire this capability and expedite rock mass characterization. Since current studies on applying deep learning to rock mass characterization are limited, this study aims to explore the feasibility of applying deep learning to characterize RQD and J_n.

2 METHODOLOGY

2.1 Overall workflow

The characterization of RQD and J_n can be regarded as a "classification" task. NGI (2015) suggests that the quotient RQD/J_n describes the relative block size of a rock mass due to different combination of joint frequency and pattern. The deep learning model's goal is to predict the combination of RQD and J_n from a rock mass's point cloud.

The quotient of RQD/J_n has to be first categorized. NGI (2015) classifies RQD into five categories, namely excellent (>90), good (75 – 90), fair (50 – 75), poor (25 – 50) and very poor (<25), and J_n into nine categories, namely massive, one joint set with/without random joints, two joint sets with/without random joints, three joint sets with/without random joints, four or more joint sets and crushed rocks. In theory, there are 45 RQD/J_n categories. The details of classification scheme will be discussed in Section 2.3.

The first step of training a deep learning model was the preparation of training dataset. However, collecting sufficient training data for each category in the field is time-consuming. It is also uncommon to find rock masses with low rock mass quality since they are typically avoided during the selection of site location in most of underground construction projects. Therefore, this study proposed a novel technique called **synthetic rock mass point cloud (SRMPC)** to generate point clouds with appearances similar to rock masses of different qualities. The details of SRMPC will be presented in section 2.2.

The second step was choosing a suitable deep learning architecture. According to a recent review of deep learning for point cloud by Guo et al. (2020), there are three major categories of deep learning architectures for point cloud classification. The first category recognizes objects by two dimensional images of a point cloud rendered at different angles (Guo et al., 2020). Classic 2D image deep learning techniques, such as convolution neural network (CNN), are applied to these images to perform classification. The main challenge of using this approach for rock mass characterization is that rock masses lack distinct outlines, and meaningful images are difficult to render. The second category converts point clouds into voxels and recognizes objects using 3D convolution (Guo et al., 2020). However, the resolution of the voxelized point cloud is often limited (order of about 64 x 64 x 64 voxels) as computational resources required increase exponentially with the resolution. Given the typical size of rock mass and spacing of discontinuities, the voxelized point cloud requires a very high resolution to capture all discontinuities, which is difficult to handle. The last category directly intakes the coordinates of a point cloud and performs classification by the spatial relationship of the points (Guo et al.,

Proceedings DOI: 10.21467/proceedings.171
ISBN: 978-81-970666-7-2

Series: AIJR Proceedings
ISSN: 2582-3922

2020). PointNet++ by Qi et al. (2017) is an example of this category and performed well in various benchmarking datasets for point cloud classification, such as ModelNet40.

After evaluating the strengths and limitations of different deep learning architectures, this study selected PointNet++ since it showed good performance when applied in different fields and could directly utilize point cloud data. The details of PointNet++ will be presented in section 2.3.3.

The last step was assessing the performance of trained deep learning models. Due to limited available real datasets, the performance of the model was evaluated quantitatively using a separated set of SRMPC, which is never seen by the model. The separated set is also used as the testing dataset during the training process. Real datasets were used to assess the performance of the model qualitatively. Details of the real datasets will be discussed in section 2.6.

2.2 Synthetic Rock Mass Point Cloud (SRMPC)

2.2.1 Overall process

The generation of synthetic rock mass point cloud (SRMPC) comprises three stages, namely discontinuity generation, point cloud generation, and attributes computation, as shown in Figure 1.

The first stage aims to create an implicit representation of a rock mass before excavation. The discontinuity generation process of SRMPC was inspired by the creation of synthetic rock mass (SRM) for numerical modelling. SRM refers to explicit jointed rock mass models using discrete fracture network (DFN) to model discontinuities (Ivars et al., 2011). A DFN specifies the location, orientation and other geometric properties of discontinuities, which can be obtained by geological mapping, stochastic generation and/or numerical simulation (Lei et al., 2017). In this study, stochastically generated discontinuities were used.

The second stage exposes the rock mass by mimicking the excavation process, allowing for point cloud generation. The "excavation" process was developed by combining geotechnical engineering experience and techniques in computer constructive solid geometry (Voelcker & Requicha, 1977). To convert the implicit representation of the rock mass into an explicit point cloud, sphere tracing, a computer graphic technique, was used.

The final stage involves computing and appending attributes to the generated point cloud for subsequent applications.

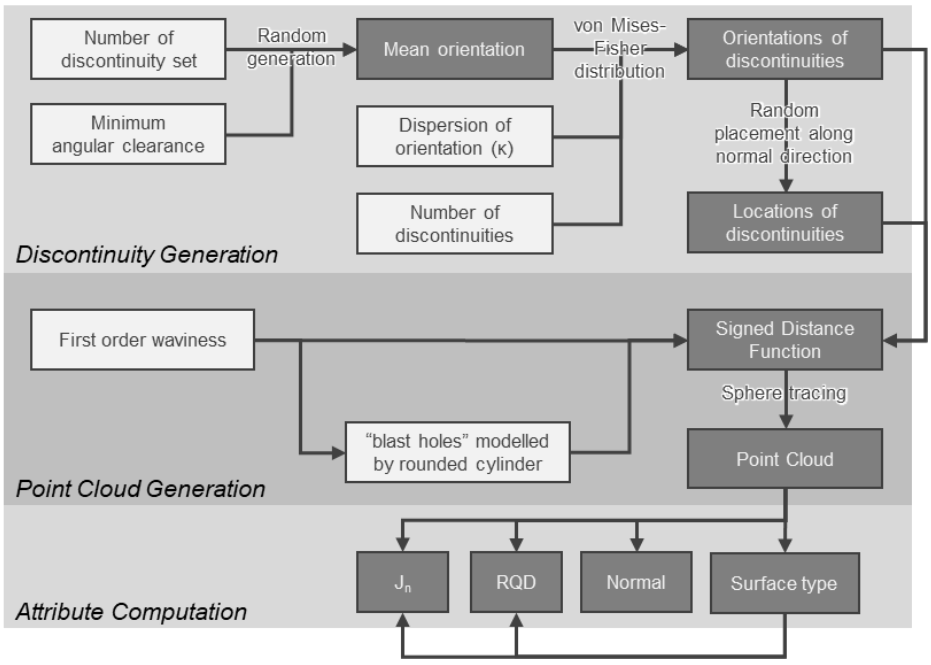

Figure 1: Workflow of generating a synthetic rock mass point cloud

2.2.2 Discontinuity Generation

The first step of generating a SRMPC is to determine the desired discontinuity pattern, including the number of discontinuity sets, number of discontinuities, angular difference between sets and dispersion of orientation within set. The von Mises-Fisher (vMF) distribution was used to generate the orientation of discontinuities, and a Poisson point process was used for determining the location of discontinuities, as the presence and spatial distribution of natural discontinuities were found to fit well with these stochastic processes (Dershowitz, 1984).

Firstly, the mean orientation of each set is picked randomly while keeping a minimum angular clearance. This ensures that different discontinuity sets can be distinguished by their orientation.

Secondly, for each discontinuity set, the orientation of individual discontinuities is generated by assuming their orientations follow the von Mises-Fisher Distribution. The generation algorithm by Hornik & Grün (2014), based on the Wood (1994)'s algorithm, was adopted in this study. To avoid excessive mixing between different discontinuity sets, the parameter of dispersion (i.e. κ) of the orientations within each set is selected randomly from a range of values based on the minimum angular clearance.

Next, as the discontinuities are assumed with infinite persistence, their position can be fixed by their distance from the origin along their normal vector. Discontinuities are randomly positioned within the specified extent. This process can recreate a discontinuity spacing pattern that generally follows the negative exponential distribution, commonly observed in real rock masses (Priest & Hudson, 1981).

2.2.3 Point Cloud Generation

The next step is to "expose" the discontinuities planes and add curved random fractures to the rock mass, simulating a blasting process. The algorithms for various 3D objects and sphere tracing were adopted and modified from Quilez (2023). First, the first order waviness of a rock mass is modelled using a cosine function. Second, rounded cylinders that mimic "blast holes" and the radial cracks generated by "blasting" are placed on the wavy surface created by the cosine function. The discontinuity planes and these cylinders are combined to form a signed distance function for the rock mass. A signed distance function provides information on the distance between the surface and the input coordinates (Quilez, 2023). Next, sphere tracing, which makes use the properties of signed distance functions to effectively render 3D geometry, is applied to produce the point cloud.

2.2.4 Attribute Computation

Lastly, the surface each ray encounters is tracked during the sphere tracing process. Attributes of that surface, including the surface type (random fractures caused by the "blast holes" or discontinuity surface) and the normal vector, are inherited to the point cloud. With these attributes, the RQD and J_n value can be obtained by volumetric joint counting (Palmstrom, 2005).

2.3 Training datasets

2.3.1 35-class classification scheme

The 35-class classification scheme is developed based on the five categories of RQD and nine categories of J_n defined in NGI (2015). In theory, the combinations of RQD and J_n represents different shapes and sizes of blocks in a rock mass, which is represented by the quotient of RQD/J_n (NGI, 2015). However, some combinations of RQD and J_n yield the same value but have different appearances. For instance, a rock mass with one joint set (J_n = 2) and an RQD of 10, and a rock mass with three joint sets and random joints (J_n = 12) and an RQD of 60, both have the same quotient value (5), but their appearances are likely to differ significantly. As the deep learning model characterizes rock mass by its appearance, the direct use of RQD/J_n as the label may confuse the deep learning model. Therefore, a categorical label instead of a numerical value was adopted. As a result, it is necessary to convert RQD into a categorical variable, and the qualitative classification scheme for RQD used by NGI (2015) is adopted.

With five classes of RQD and nine classes of J_n, there are 45 possible RQD/J_n combinations. Upon examining these combinations, it was discovered that some of them are rare or not possible, such as crushed rock mass with excellent RQD, and some combinations have similar appearances, such as crushed rock and rock mass

Proceedings DOI: 10.21467/proceedings.171
ISBN: 978-81-970666-7-2

Series: AIJR Proceedings
ISSN: 2582-3922

with four or more joints sets with very poor RQD. As such, some of these 45 classes are removed and grouped, resulting in a 35-class classification scheme. The RQD/J_n of each class is shown in Figure 2 : RQD/J_n value of the 35-class classification scheme.Figure 2.

J_n / RQD	Massive (0.5 – 1.0)	One joint set (2)	One joint set + random (3)	Two joint set (4)	Two joint set + random (6)	Three joint set (9)	Three joint set + random (12)	Four or more joint sets (15)	Crushed rock (20)
Excellent (> 90)	95	48	32	24	16	11	8		
Good (75 – 90)		41	28	21	14	9	7	6	
Fair (50 – 75)		31	21	16	10	7	5	4	
Poor (25 – 50)		19	13	9	6	4	3	3	
Very Poor (<25)		6	4	3	2	1.4	1.0	0.8	0.6

Figure 2 : RQD/J_n value of the 35-class classification scheme.
Very poor rock masses with four or more joint sets and crushed rock (highlighted in orange) are considered as one class in this scheme.

2.3.2 20-class classification scheme

After experimenting the 35-class classification scheme (details will be discussed in 3.1), it was noted some classes in the 35-class classification scheme had similar appearances, in particular rock masses with the same number of major joint sets but with and without random joints. The deep learning model struggled to distinguish between these classes. Since a reasonably high accuracy is essential for practical applications, a simplified 20-class classification scheme was developed to improve accuracy. As random joints are generally limited in number and have a minimal impact on the rock mass's appearance, the J_n classes with and without random joints are combined. For example, a rock mass with one discontinuity set and another with one discontinuity set plus random discontinuity are considered the same in this scheme. In practice, the J_n value can be conservatively taken as that with the random discontinuity sets, as shown in Figure 3. This scheme reduces the task's difficulty while maintaining applicability in practical scenarios.

J_n / RQD	Massive (0.5 – 1.0)	One joint set (2)	One joint set + random (3)	Two joint set (4)	Two joint set + random (6)	Three joint set (9)	Three joint set + random (12)	Four or more joint sets (15)	Crushed rock (20)
Excellent (> 90)	95	32		16		8			
Good (75 – 90)		28		14		7		6	
Fair (50 – 75)		21		10		5		4	
Poor (25 – 50)		13		6		3		3	
Very Poor (<25)		4		2		1.0		0.6	

Figure 3: RQD/J_n value of the 20-class classification scheme

2.3.3 Generation of training dataset

The following process was adopted to produce a balanced dataset with an equal number of instances in each class. For both classification schemes, a total of 300 instances for each class were generated.

First, a large number of point clouds are generated for each J_n class, with a randomly picked number of discontinuities. During point cloud generation, some generated discontinuity planes may not be exposed due to their locations, orientations, and density and sizes of "blast holes". As a result, the number of discontinuities

and discontinuity sets subsequently shown in the SRMPC is usually less than the targeted number. A large number of SRMPCs with ranges of targeted properties were generated, and the actual class that each SRMPC belongs to was determined.

The previous step was repeated for classes with fewer number of instances than the target (i.e. 300). On the other hand, if there were more instances than the target, the desired number of instances were picked randomly.

The training dataset for the 20-class classification scheme was prepared from that for the 35-class classification scheme through random selection. As the classes with and without random joints are combined in the 20-class classification scheme, 150 point clouds with random joints and 150 point clouds without random joints were randomly selected to form the combined class.

2.4 Model architecture

After reviewing some well-known point cloud classification architectures, PointNet++ by Qi et al. (2017) was chosen for this study. The primary reason is that it is capable to cope with point clouds with a large number of points and has many previous studies demonstrating its performance in classification.

Since most available pre-trained PointNet++ models (e.g. Yan, 2019) were trained for classifying objects with distinct outlines, such as a desk or a chair, and used point clouds with relatively few points (<10,000 points), it was considered that these pre-trained models could not be applied directly to rock mass characterization. Therefore, this study trained the deep learning model from scratch with randomly initialized parameters.

Compared to the original structure of PointNet++, the number of input points was increased to 10,000, and the output class was changed to 35 or 20, depending on the adopted classification scheme. The layers in between remain unmodified.

2.5 Model training

The training dataset was first randomly split into training and testing datasets with an 80:20 ratio (i.e 240 samples for training and 60 samples for testing). The total numbers of training samples and testing samples were 8,400 and 2,100 respectively, for the 35-class classification scheme, and 4,800 and 1,200 respectively for the 20-class classification scheme.

Before feeding the data into the model, pre-processing including subsampling, random rotation, random shift and jittering, was carried out at the beginning of each epoch. Each SRMPC in the training and testing dataset was a 3 m x 3 m x 3 m rock mass with about 40,000 points. Each SRMPC was randomly subsampled to 10,000 in every epoch. The training data was then rotated, shifted and jittered to further augment the data, while the testing data remained unmodified. This process aimed to simulate variations in field data collection to make the synthetic data more realistic. An example of data augmentation is shown in Figure 4.

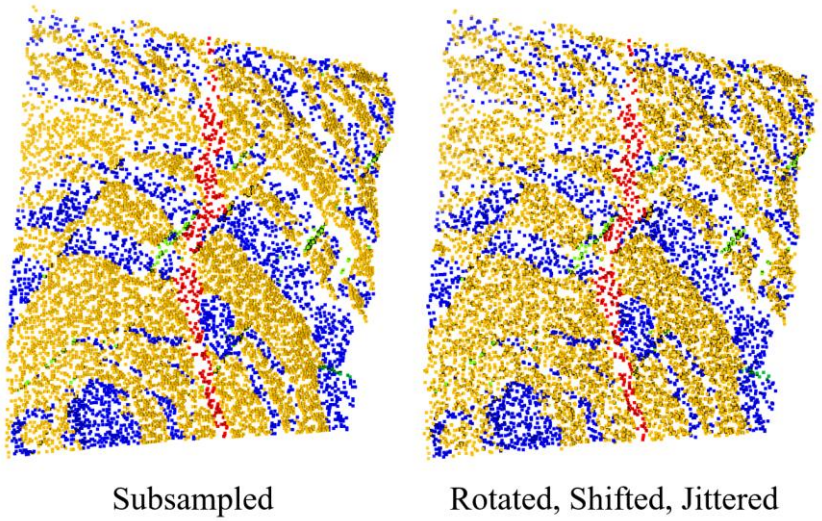

Figure 4: Data augmentation applied on the training data. The colors denote the surface types and are shown for illustration purposes. The information of surface type is not included in the training data.

Proceedings DOI: 10.21467/proceedings.171
ISBN: 978-81-970666-7-2

Series: AIJR Proceedings
ISSN: 2582-3922

An implementation of PointNet++ in PyTorch (Paszke et al., 2019) developed by Yan (2019) was adopted for training the deep learning models in this study. A total of 200 epochs of training was performed for both the 35-class and 20-class classification schemes. The hyperparameters adopted for the training of deep learning models in this study are shown in Table 1. Since the initial focus of this study was to explore the feasibility of applying deep learning for rock mass characterization, fine-tuning of these hyperparameters was not carried out. It was anticipated that the difference caused by fine-tuning is likely limited.

Table 1: Hyperparameters adopted for training the deep learning models

Hyperparameters	**Value**
Epoch	200
Batch size	36
Optimizer	Stochastic gradient descent
Learning rate	0.01
Momentum	0.9

2.6 Evaluation

The performance of the deep learning models was evaluated both quantitatively and qualitatively. Due to limited variations of rock mass quality in real datasets, it is difficult to evaluate the model quantitatively with real datasets. Instead, the synthetic testing dataset was used for quantitatively assessing the performance.

The real datasets were retrieved from the Geotechnical Engineering Office, Civil Engineering and Development Department of the Hong Kong Special Administrative Region Government (GEO, 2021), which were released under the benchmarking exercise for rock mass discontinuity survey. These datasets include the point cloud of an abandoned quarry face (Feature No. 11SE-B/C249**Error! Reference source not found.**) l ocated at Lei Yue Mun Point and the point cloud of a rock slope (Feature No. 11NW-D/C80**Error! Reference source not found.**) located at Shun Yung Street, Ho Man Tin.

These real datasets contain noises, such as vegetation, since they were acquired on the surface rather than underground. Portions with little vegetation and rock mass with clear exposures were extracted for evaluation to minimize the impact caused by these noises.

Furthermore, real point clouds, including those used for verification, are usually larger than that of the training data (i.e. 3 m x 3 m x 3 m). As such, a sliding window approach was adopted (Figure 5). The input point cloud is first dissected into 1 m x 1 m x 1 m cells. For each cell, the surrounding neighbouring cells (i.e. 26 cells) are selected together to form a 3 m x 3 m x 3 m window. The prediction result of the deep learning model is written to the points in that 1 m x 1 m x 1 m cell at the centre. This ensures the model makes predictions using the same scale as the training data, while the variation of a rock mass can also be shown.

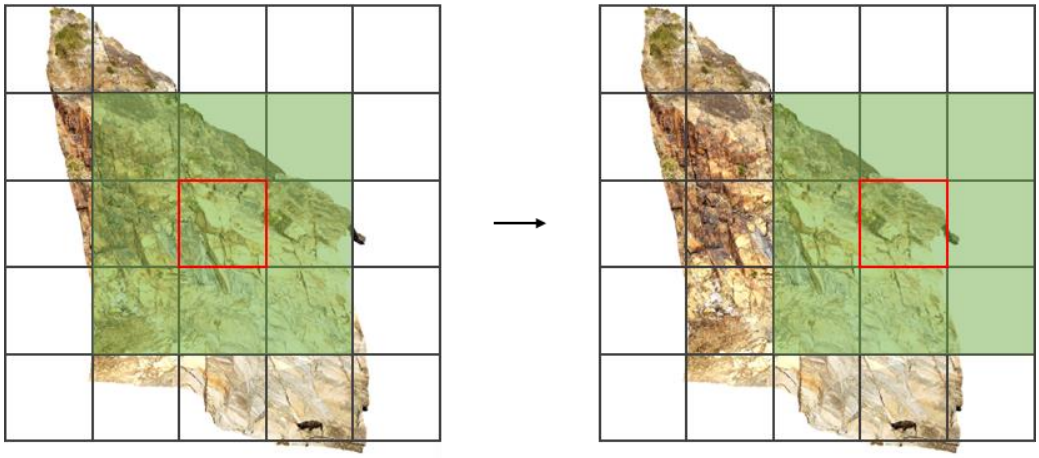

Figure 5: Schematic diagram of the sliding window approach adopted

3 RESULT AND DISCUSSION

3.1 35-class classification scheme

3.1.1 Quantitative results

The results demonstrated that deep learning has the potential to perform rock mass characterization. Figure 6 shows the evolution of classification accuracies of the training and testing data over the 200 epochs, with the best testing accuracy achieved was 29.3%. Figure 7 shows the confusion matrix for testing data.

Firstly, the evolutions of accuracies for both training and testing datasets (Figure 6) were similar, increasing rapidly in the first few epochs and gradually stabilizing at slightly below 30%. This probably indicates that the model did not overfit and successfully learned the features of different rock masses. The relatively low accuracy may suggest that the model struggled to learn the differences between many of the classes, as shown in the confusion matrix (Figure 7).

Secondly, apart from examining the combination of RQD and J_n as a whole, it is also possible to assess the performance in distinguishing different J_n and RQD values. Regarding the performance of classifying different J_n value, the confusion matrix (Figure 7) showed that the model is capable of distinguishing different numbers of major joint sets when the RQD lower than "excellent" (i.e. there are certain number of discontinuities). Nevertheless, the model performed less satisfactory in distinguishing the presence of random sets. One of the possible reasons is that deep leaning models perform classification primarily based on low-frequency signals (i.e. overall appearance of the point cloud). When there are few discontinuities or the presence of random discontinuities, the overall outlook of the rock mass may be very similar. For a human, an engineering geologist will examine the surroundings and make measurements to identify the major discontinuity sets in these cases. On the other hand, when there are a certain number of discontinuities, different numbers of major joint sets usually result in very different block shapes, for example, rock mass with one major discontinuity set (e.g. sedimentary rock) forms layers and rock mass with three orthogonal discontinuity sets forms cubes. The deep learning model is capable of distinguishing these patterns.

Thirdly, regarding the performance of classifying different RQD values, the confusion matrix showed that the model is capable of distinguishing rock mass with good and poor RQD with limited precision, for example, a rock mass with fair RQD is often misidentified as good or poor. One of the possible reasons is that RQD is a continuous variable and the adopted classification was arbitrary, such that rock mass with similar RQD can be classified into two different classes. Nevertheless, for a human to deduce a precise RQD (in the order of 5), it requires a technique including volumetric joint counting and empirical correlation. It appears to be difficult for the computer to develop such a strategy without explicitly incorporating that into the model architecture.

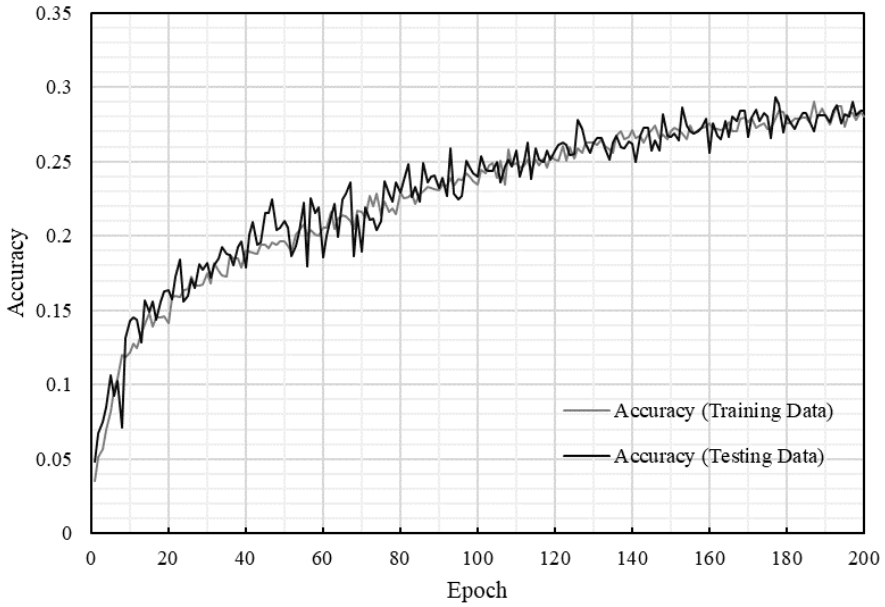

Figure 6: Classification accuracy of training and testing data (35-class classification scheme)

Proceedings DOI: 10.21467/proceedings.171
ISBN: 978-81-970666-7-2

Series: AIJR Proceedings
ISSN: 2582-3922

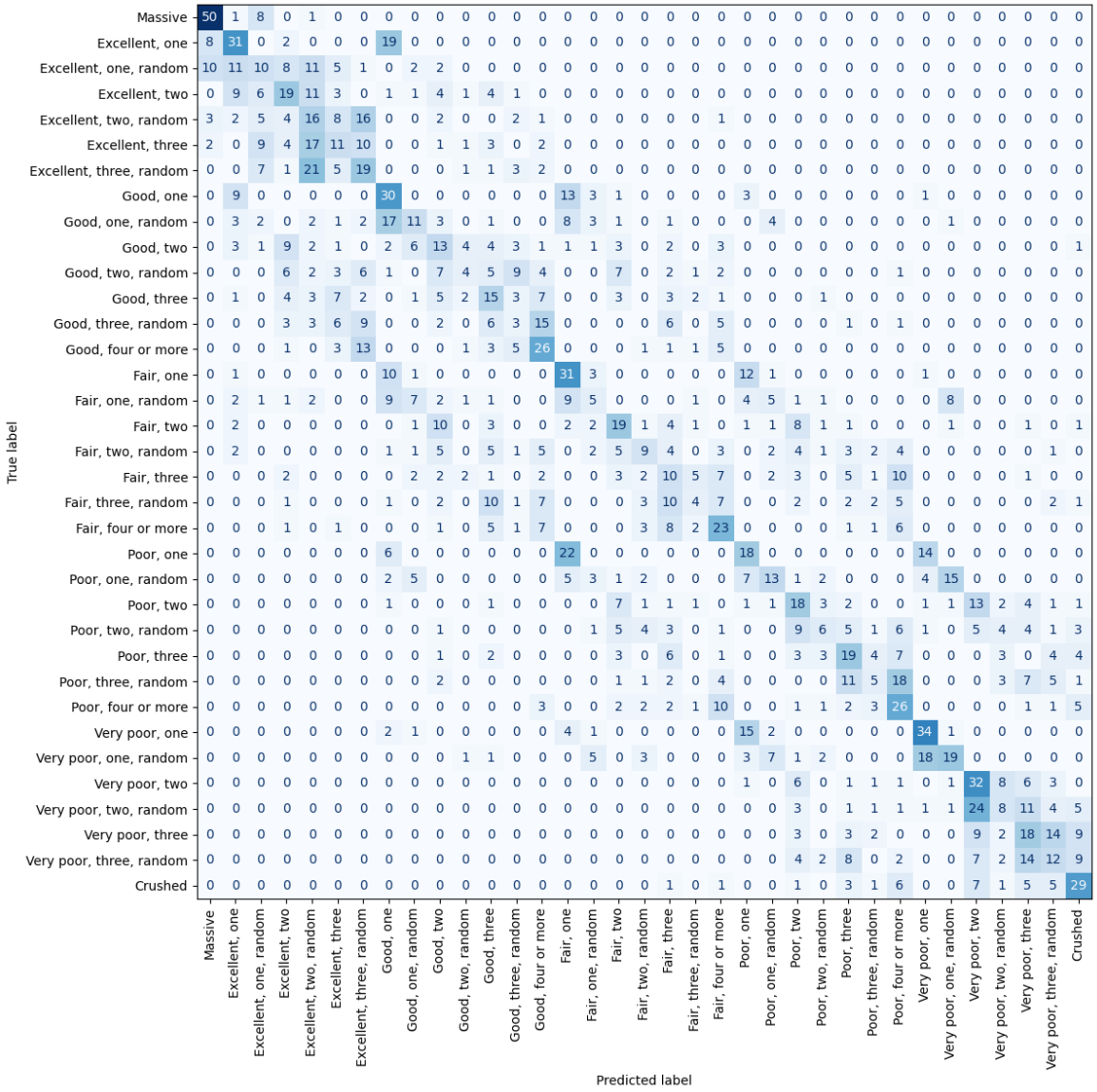

Figure 7: Confusion matrix of testing data (35-class classification scheme). Numbers in the cell denote the number of different combinations of true labels and predicted labels.

3.1.2 Qualitative results

The prediction of RQD/J_n class of Feature Nos. 11SE-B/C249 and 11NW-D/C80 are shown in Figure 8 and Figure 9. The predictions are generally in line with the observations in the field mapping done by GEO (2021).

Field mapping conducted by GEO (2021) identified four major discontinuity sets with spacing between 0.5 m and 1 m in the rock mass of Feature No. 11SE-B/C249. Palmstrom (2005) suggested that the volumetric joint count can be estimated from the joint spacing. In this case, the volumetric joint count (J_v) of the rock mass is around 6 m^{-3}. Next, based on the empirical correlation between volumetric joint count and RQD, proposed by Palmstrom (2005) and also suggested in NGI (2015), the RQD of the rock mass is approximately 95 (i.e. "excellent").

For Feature No. 11SE-B/C249, the RQD/J_n predicted by the deep learning model is broadly consistent with the manual observations by GEO (2021). As shown in Figure 8, the subhorizontal joint set exposes in gentler areas and the rock mass is apparently massive, the deep learning model also predicted those generally as "massive". On the other hand, the deep learning model predicted the steeper areas generally as two different classes, namely "rock mass with excellent RQD and three joint sets with random joints" and "rock mass with good RQD and four or more major joint sets". The model predicted the areas with fewer joints as classes with fewer major discontinuity sets, possibly because the deep learning model may have misidentified the fourth

major joint set as random discontinuities. For corners or protruding parts of the rock mass, the model predicted these areas as rock mass with poorer RQD with fewer major joint sets, probably because a smaller rock mass was actually included in the 3 m x 3 m x 3 m.

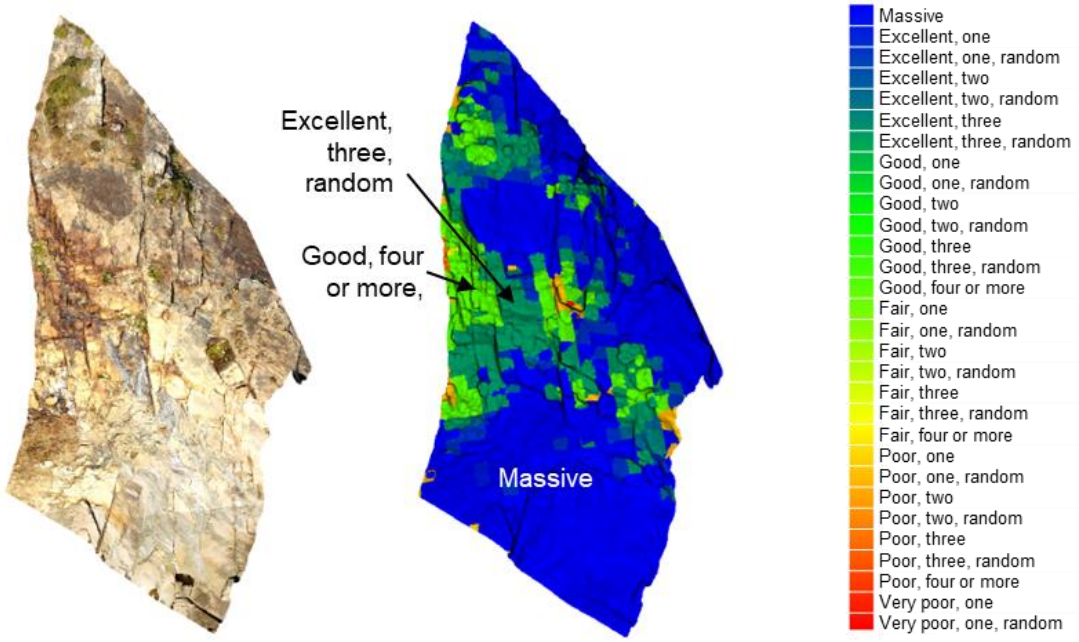

Figure 8: Prediction of RQD/J_n of Feature No. 11SE-B/C249 by the deep learning model

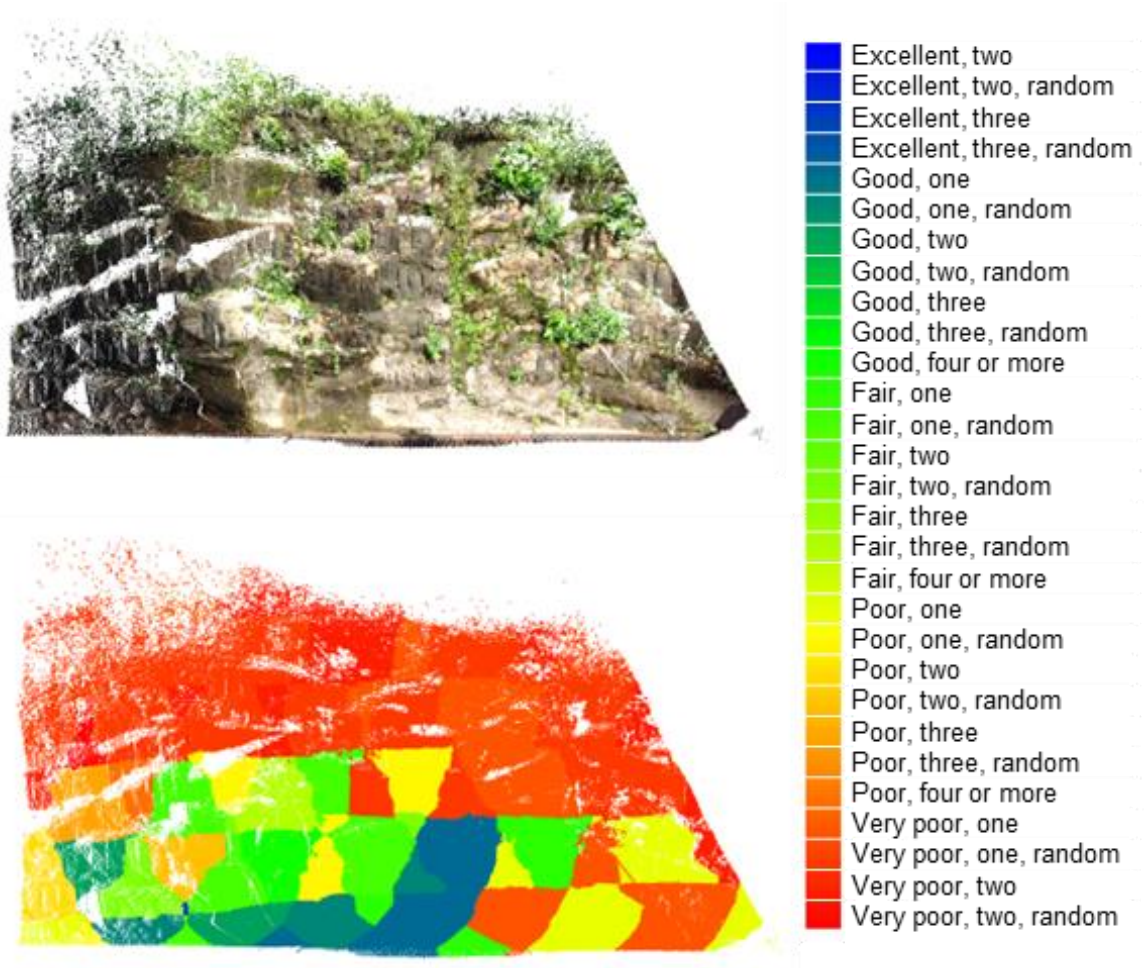

Figure 9: Prediction of RQD/J_n of Feature No. 11NW-D/C80 by the deep learning model

Proceedings DOI: 10.21467/proceedings.171
ISBN: 978-81-970666-7-2

Series: AIJR Proceedings
ISSN: 2582-3922

For Feature No. 11NW-D/C80, GEO (2021) also identified four major joint sets, but with a smaller spacing between 0.3 m to 1 m (GEO, 2021). Using the previously approach, J_v of the rock mass is approximately 7.5 m^{-3}, and the RQD is about 90, which falls between "excellent" and "good" classifications.

The RQD/Jn predicted by the deep learning model broadly aligns with the manual observations by GEO (2021). As shown in Figure 9, there is vegetation in the upper part of the rock mass and the model predicted that area as "rock mass with very poor RQD and one major joint set and random joints". On the other hand, the model classified the lower part of the rock mass having one major joint set with/without random joints with RQD between good and poor. Although four major joint sets are presence in the rock mass, only the persistent subhorizontal joint set is well exposed in the lower part of this portion of rock mass. Subvertical joint sets are poorly exposed and may be regarded as "random joints" by the model.

Furthermore, the lower part of the rock mass is also characterized by pre-splitting surfaces, which are subparallel to the slope surface and planar in nature. While these pre-splitting surfaces may resemble discontinuity planes, the model did not seem to count these surfaces as one of the major joint sets. It appears that the model can differentiate between pre-splitting surfaces and natural discontinuity planes; however, further evidence and tests are necessary to confirm whether the model has truly learnt the differences between these two surface types.

3.2 20-class classification scheme

The 20-class classification scheme exhibits an improved classification accuracy of about 44.2%. Figure 10 shows the confusion matrix for the testing data. The model shows better accuracy in classifying rock masses with different J_n classes. The simplified J_n classes may enable the model to focus on learning features created by different numbers of major discontinuity sets. The improvement also indicates that deep learning models perform more robustly when carrying out relatively coarse-grained classification.

However, the model still has relatively low precision in predicting RQD classes, which limits the improvement in classification accuracy. The simplification of J_n classes does not significantly improve the model's capability to distinguish rock masses with different RQD values. As a result, the practical usage of these deep learning models remains limited.

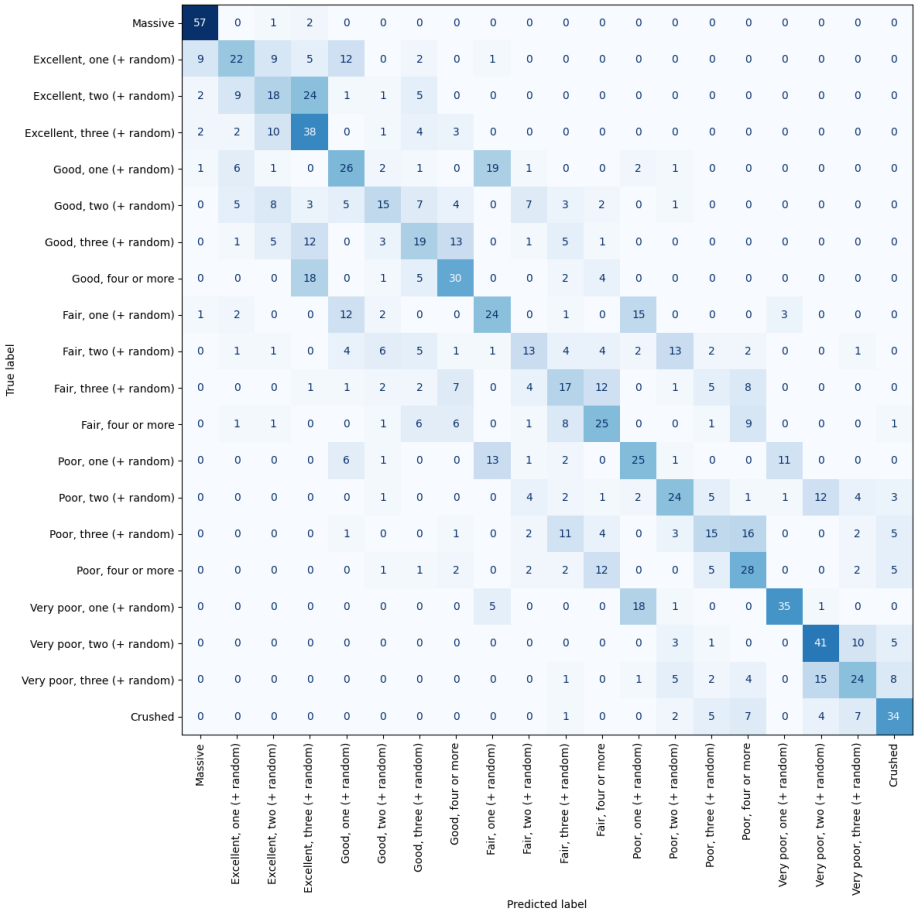

Figure 10: Confusion matrix for testing data (20-class classification scheme). Numbers in the cell denote the number of different combinations of true labels and predicted labels.

3.3 Other observations

During the preparation of training dataset, it was observed that some classes are challenging to generate using the SRMPC algorithm. For example, rock masses with one discontinuity set and very poor RQD were difficult to generate because closely spaced discontinuities are not easily exposed at the resolution of SRMPC. Increasing the resolution of random fractures and the point cloud could alleviate this issue. However, doing so would not only increase generation time, but also raise the requirements for acquiring real data since the resolution of SRMPC was set to be similar to that of typical equipment.

3.4 Synthetic Rock Mass Point Cloud

The results above have demonstrated the feasibility of using synthetic data to train a deep learning model and apply it to real dataset. The SRMPC not only aids in applying deep learning to rock mass characterization, but also supports other machine learning applications in rock mechanics, since a large amount of data with known discontinuity properties can be generated quickly. For example, the SRMPC can be combined with numerical modelling to explore the possibility of predicting stability analysis results based on point cloud data.

3.5 Way forwards

Firstly, classification-based approach can be further explored. State-of-the-art model architectures or pre-trained models, trained with very large datasets, can be adopted. In other fields of machine learning, such as computer vision, “transformer” models trained with vast datasets have become increasingly powerful. For example, the DINOv2 model, trained with an image dataset containing about 142 million images (LVD-142M), exhibited strong performance across various tasks, including image classification, segmentation and monocular depth

Proceedings DOI: 10.21467/proceedings.171
ISBN: 978-81-970666-7-2

Series: AIJR Proceedings
ISSN: 2582-3922

estimation (Oquab et al., 2023). When a similar model for performing 3D tasks released in the future, it will be worthwhile to further investigate the classification-based approach.

Secondly, performing discontinuity extraction using a deep learning model can be investigated. In this study, one of the limitations observed in deep learning models is their relatively weak performance in fine-grained interpretation, such as distinguishing the presence of random discontinuities. Deep learning models can first be used to extract all discontinuity planes (i.e., obtaining the complete geometric data), and then RQD and J_n classes can be computed similarly to the existing methods mentioned previously. The extracted discontinuity planes by the deep learning models could potentially also be used in other rock mass classification systems and the generation of DFN models.

4 CONCLUSIONS

This study has demonstrated the potential of deep learning in rock mass characterization. Deep learning models can perform rock mass characterization quickly with fair precision. A simplified 20-class model was also tested, which improved the accuracy but not to a level high enough to be deployed into routine construction workflows. Further research is needed to practically adopt deep learning for routine rock mass characterization. Last but not least, a novel solution called SRMPC was developed in this study to address the scarcity of training data, proving useful for deep learning in rock mass characterization. It also holds potential for application in other machine learning tasks within the field of geological engineering.

ACKNOWLEDGEMENTS

The findings in this paper were based on the Master dissertation of Mr. K.K. CHAN, supervised by Prof. Louis N.Y. WONG at The University of Hong Kong, and a project carried out by the Geotechnical Engineering Office. The authors also gratefully acknowledge the valuable experience from related studies carried out in the Geotechnical Engineering Office. This paper is published with the permission of the Head of the Geotechnical Engineering Office and the Director of Civil Engineering and Development, the Government of the Hong Kong Special Administrative Region.

HOW TO CITE

Wong *et al.* (2024). Exploring Computer-based Rock Mass Characterization. *AIJR Proceedings*, 284-297. https://doi.org/10.21467/proceedings.171.25

REFERENCES

Barton, N., Lien, R. & Lunde, J. 1974. Engineering classification of rock masses for the design of tunnel support. *Rock Mechanics*, 6: 189–236.

Barton, N. 2015. Forty Years with the Q-system – Lessons and Developments. Keynote Paper. Institute of Materials, Minerals and Mining, Hong Kong Branch.

Chen, J., Zhu, H., & Li, X. 2016. Automatic extraction of discontinuity orientation from rock mass surface 3D point cloud. *Computers & geosciences*, 95: 18–31

Dershowitz, W. S. 1984. Rock joint systems. Massachusetts Institute of Technology. PhD thesis.

GEO. 2021. Review of Benchmarking Exercise on Digital Rock Mass Discontinuity Survey 2020.

Gigli, G., & Casagli, N. 2011. Semi-automatic extraction of rock mass structural data from high resolution LIDAR point clouds. *International journal of rock mechanics and mining sciences (Oxford, England : 1997)*, 48: 187–198.

Guo, Y., Wang, H., Hu, Q., Liu, H., Liu, L., & Bennamoun, M. 2020. Deep learning for 3d point clouds: A survey. *IEEE transactions on pattern analysis and machine intelligence*, 43(12): 4338-4364.

Hornik, K., & Grün, B. 2014. movMF: An R package for fitting mixtures of von Mises-Fisher distributions. *Journal of Statistical Software*, 58(10): 1-31.

Ivars, D.M., Pierce, M.E., Darcel, C., Reyes-Montes, J., Potyondy, D.O., Young, R.P., & Cundall, P.A. 2011. The synthetic rock mass approach for jointed rock mass modelling. *International Journal of Rock Mechanics and Mining Sciences*, 48: 219–244.

Lei, Q., Latham, J.P., & Tsang, C.F. 2017. The use of discrete fracture networks for modelling coupled geomechanical and hydrological behaviour of fractured rocks. *Computers and Geotechnics*, 85: 151-176.

NGI. 2015. Using the Q-system: Rock Mass Classification and Support Design (handbook). Norwegian Geotechincal Institute, Oslo.

Oquab, M., Darcet, T., Moutakanni, T., Vo, H., Szafraniec, M., Khalidov, V., Fernandez, P., Haziza, D., Massa, F., El-Nouby, A., Assran, M., Ballas, N., Galuba, W., Howes, R., Huang, P.Y., Li, S.W., Misra, I., Rabbat, M., Sharma, V., … Bojanowski, P. 2023. DINOv2: Learning Robust Visual Features without Supervision (arXiv:2304.07193). *arXiv*. http://arxiv.org/abs/2304.07193

Palmstrom, A. 2005. Measurements of and correlations between block size and rock quality designation (RQD). *Tunnelling and Underground Space Technology*, 20(4): 362–377.

Paszke, A., Gross, S., Massa, F., Lerer, A., Bradbury, J., Chanan, G., Killeen, T., Lin, Z., Gimelshein, N., & Antiga, L. 2019. Pytorch: An imperative style, high-performance deep learning library. *Advances in Neural Information Processing Systems*, 32.

Priest, S. D., & Hudson, J. A. 1981. Estimation of discontinuity spacing and trace length using scanline surveys. *International Journal of Rock Mechanics and Mining Sciences & Geomechanics Abstracts*, 18(3): 183–197.

Qi, C.R., Yi, L., Su, H., & Guibas, L.J. 2017. Pointnet++: Deep hierarchical feature learning on point sets in a metric space. *Advances in Neural Information Processing Systems*, 30.

Quilez, I. 2023. Inigo Quilez. https://iquilezles.org/.

Riquelme, A.J., Abellán, A., Tomás, R., & Jaboyedoff, M. 2014. A new approach for semi-automatic rock mass joints recognition from 3D point clouds. *Computers & geosciences*, 68: 38–52.

So, A.C.T., Leung W.K., & Wong J.C.F. 2021. A Novel Method for Measurement of Orientation of Rock Joints from Point Cloud by Facet Amalgamation Approach. The 42nd Asian Conference on Remote Sensing (ACRS2021) 22-24th November, 2021 in Can Tho University, Can Tho city, Vietnam.

Voelcker, H., & Requicha, A. 1977. Constructive solid geometry. University of Rochester.

Wood, A.T. 1994. Simulation of the von Mises Fisher distribution. *Communications in statistics-simulation and computation*, 23(1): 157-164.

Yan, X. 2019. Pointnet/Pointnet++ Pytorch [Python]. https://github.com/yanx27/Pointnet_Pointnet2_pytorch

Proceedings DOI: 10.21467/proceedings.171
ISBN: 978-81-970666-7-2

Series: AIJR Proceedings
ISSN: 2582-3922